COMMUNICATION

Promoting high T_2 contrast in Dy-doped MSNs through Curie effects

Received 00th January 20xx,
Accepted 00th January 20xx

DOI: 10.1039/x0xx00000x

Connor M. Ellis,[a] Juan Pellico,[a,b] Liam A.J. Young,[c,d] Jack Miller,[c,d,e] and Jason J. Davis*[a]

Contrast agents retaining high relaxivities at ultrahigh magnetic fields underpin an enhanced image sensitivity within derived MRI scans. By varying the Dy^{3+} loading density inside a mesoporous silica architecture the dominant Curie effect can be effectively tuned so as to optimise T_2 contrast at magnetic fields as high as 11.7 T.

Magnetic Resonance Imaging (MRI) provides non-invasive, whole-body, high-resolution, 3D images of human tissues. Although routinely applied clinically, it is intrinsically insensitive, an issue underpinning a drive to higher scanner static magnetic field strengths. The controlled application of exogenous contrast agents can provide complementary information about biological processes (such as fibrosis), or more generally to increase signal-to-noise in images, improving scan sensitivity.[1–3] Agents capable of supporting efficient proton relaxation at increasingly high magnetic fields are highly desirable, but comparatively rare. Under such circumstances, negative, or T_2 contrast agents, are more suitable since the performance of positive, or T_1 contrast agents, decreases with increasing field strength.[4–6] Of the T_2 candidates, Dy^{3+} possesses the highest effective moment (μ_{eff} = 10.6 μ_{B}) and the shortest electronic relaxation time (~ 10^{-13} s) of the lanthanide ions, and is particularly effective at promoting protic relaxation at high magnetic fields.[7] A number of Dy-based chelated complexes have been synthesised and analysed to date; these exhibit moderate transversal relaxivity (r_2) values at high (> 3.0 T) or ultra-high (≥ 7 T) magnetic fields but suffer from short blood circulation times.[8–11] To overcome this issue, nanoparticles have been proposed as a scaffold to support Dy^{3+} ions where the combined effects of rotational correlation and high local concentration (together with a synthetic versatility leading to the possibility of functionalisation) are notable.[12] Initial approaches to this have included the production of inorganic Dy_2O_3, DyF_3, $NaDyF_4$ or Dy-doped $MnCO_3$ nanocrystals of varying size and shape, some with T_2 relaxivities exceeding 300 mM^{-1} s^{-1} at 9.4 T.[13–16] Additionally, Dy-DOTA complexes have been incorporated into the Tobacco Mosaic Virus (TMV) nanoparticles or Mesoporous Silica Nanoparticles (MSNs) where, again, high r_2 relaxivities have been noted at fields exceeding 9 T.[17–19] Interestingly, in the latter work, a linear increase in relaxivity with the square of the magnetic field is observed, consistent with a dominant outer-sphere (OS) Curie mechanism of relaxation, an observation recently mirrored with Dy-DOTA doped MSNs,[20] and in strong contrast to the dominance of inner-sphere (IS) contribution for molecular Dy-complexes.[8] There are, then, indications that nanoscale confinement diminishes the contributions by the inner-sphere in favour of those of the outer-sphere. Herein we set out to engineer and optimise the T_2 contrast generated by Dy-loaded nanoparticles by specifically utilising both the effects of nanochannel-confined water and optimising Curie effects through loaded Dy-density.

The dominant outer sphere relaxation is comprised of both dipolar ($R_{2\text{D}}^{\text{OS}}$) and Curie terms ($R_{2\text{C}}^{\text{OS}}$), with the latter contribution significant for paramagnetic species with short electronic relaxation times and shown to scale linearly with B_0^2.[21] Curie spin effects are, then, important at high fields (or when rotational correlation times are long).[8,17] These effects are dipolar in origin and arise from the polarisation of a large electron spin population with an applied field.[22] The generated net macroscopic magnetisation ($\langle S_z \rangle$) can interact with nuclear magnetic dipoles through dipolar coupling, the effect being modulated by molecular tumbling and resulting in a nuclear-spin relaxation pathway that can significantly impact T_2.[23,24] Since the absolute value of $\langle S_z \rangle$ should increase with loading density, we set out here to demonstrate an ability to tune transverse relaxation at the point of synthesis, and, in so doing, generate Dy-doped MSNs that exhibit strong T_2 responses that scale with engineered Curie effects. To probe Curie spin contributions, across different particle compositions, AC magnetic susceptibility analyses were used. These are

[a] Department of Chemistry, University of Oxford, South Parks Road, Oxford, OX1 3QZ, UK. E-mail: jason.davis@chem.ox.ac.uk; Fax: +44 (0)1865 272 690; Tel: +44 (0)1865 275 914
[b] School of Biomedical Engineering & Imaging Sciences, King's College London, St. Thomas' Hospital, London, SE1 7EH
[c] Department of Physiology, Anatomy & Genetics, University of Oxford, South Parks Road, Oxford, OX1 3PT, UK
[d] Oxford Centre for Clinical Magnetic Resonance Research, Radcliffe Department of Medicine, University of Oxford, Level 0, John Radcliffe Hospital, Oxford, OX3 9DU, UK
[e] Department of Physics, Clarendon Laboratory, Parks Road, Oxford, OX1 3PU, UK
† Electronic Supplementary Information (ESI) available: See DOI: 10.1039/x0xx00000x

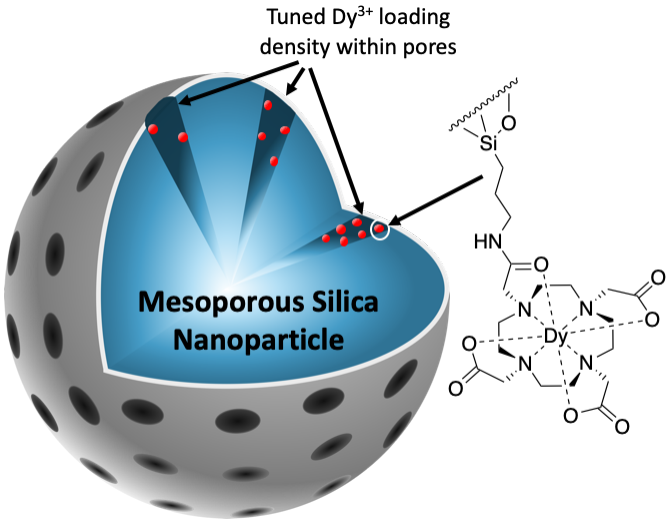

Figure 1. A schematic representing the loading of Dy-DOTA moieties within the pore channel of the silica nanoparticles. A long delay co-condensation reaction was employed to functionalise the Dy-DOTA moieties in the outer pore channel of the particles.

conducted by applying an oscillating magnetic field and associated magnetisation to investigate interacting spins within a solid.[25,26] The resolved AC susceptibility (χ_{AC}) is composed of both in-phase (χ') and out-of-phase (χ'') components that show a divergence with frequency that is dependent on the magnetic order present within the sample. This, then, reports on the spin-spin interactions (and Curie effects) that fundamentally determine T_2.[26–29] Herein we show that these effects scale with paramagnet loading density within a mesoporous silica scaffold in a manner that directly tunes Curie promoted image contrast.

The MSNs herein were synthesised by a brief modification of the Stöber method. A long delay co-condensation reaction was employed to introduce amino anchor points in the outer pore channel, to which an activated ester of 1,4,7,10-tetraazacyclododecane-1,4,7,10-tetracetic acid (DOTA) was tethered, producing DOTA-MSNs. Subsequent metalation with $DyCl_3.6H_2O$ produced the desired Dy-MSNs as reported in previous work and described in the ESI (ESI 1).[17,†] The particles exhibited high colloidal stability and a uniform size distribution (PDI < 0.1), as confirmed by dynamic light scattering (DLS) measurements, with an average hydrodynamic size of 70.7 ± 7 nm for the Dy-loaded MSNs, and no significant differences (two-tailed t-test, P > 0.05) between different Dy^{3+} loading formulations (ESI 2 & ESI 3). Transmission electron microscopy (TEM) analyses confirmed good levels of dispersion and particle uniformity (ESI 4), with an associated particle diameter of 51.8 ± 6 nm (averaged over 50 particles). The native MSNs displayed positive ζ-potential values, with an average value of 41.4 ± 0.8 mV, which then decreased after the addition of DOTA with the DOTA-MSNs exhibiting a ζ-potential of 23.8 ± 0.9 mV (ESI 2, ESI 3). This is reflective of the high amination percentage of the native MSNs (10%) which is then tethered to DOTA, reducing the ζ-potential value due to a reduction in free amine functional groups in addition to the introduction of carboxylic acid moieties present in DOTA. The final Dy-MSNs displayed a mean ζ-potential of 35.5 ± 3 mV, reflective of the incorporation of Dy^{3+} within the macrocyclic host. ATR-IR was employed to confirm the removal of the (toxic) surfactant template (CTAB; ESI 5), where the characteristic Si-O-Si stretch can be observed at 1070 cm^{-1}, with the removal of CTAB confirmed by the absence of a stretch at 2950 cm^{-1}. To quantify the Dy-loading, inductively coupled plasma mass spectrometry (ICP-MS) measurements were conducted, with the concentration of Dy^{3+} dopant varying from 0.013 mM to 0.188 mM. Control reactions for the native NH_2-MSNs with $DyCl_3.6H_2O$ (i.e., in the absence of DOTA) confirmed (ICP-MS) the absence of physisorbed Dy^{3+}, with > 98.5 % of Dy^{3+} ions chelated. The number of Dy^{3+} atoms per MSN was estimated to be tuned from 770 to 12,000 Dy^{3+} (ESI 6).[30]

Figure 2 shows the measurements for the associated transverse relaxation rate ($R_2 = 1/T_2$), and the AC susceptibility determined temperature of divergence (included as an insert), for the Dy-doped MSNs across a range of loading densities. Since a single localised spin should respond to an oscillating magnetic field, the existence of a divergence temperature is indicative of spin interactions and scales linearly with the magnitude of the loading density (there is a 75 % increase in the temperature of divergence between the recorded values for the lowest and highest loading densities) in a manner that very directly impacts the relaxation rate recorded at 11.7 T. An analysis of relaxivity per particle highlights clearly, the effects of Dy^{3+} loading density where individual particle relaxivities ranged from (2.1 ± 0.2) x 10^7 mM^{-1} s^{-1} to (7.0 ± 1.5) x 10^7 mM^{-1} s^{-1} (ESI 8) as Curie contributions scale and there is an increased dephasing of protic spin. This translates to equivalent enhancements in image contrast supported at progressively lower particle concentrations as loading density increases.

To demonstrate an extension of this high and tuneable relaxation to clinical imaging, we assessed the effect of Dy^{3+}

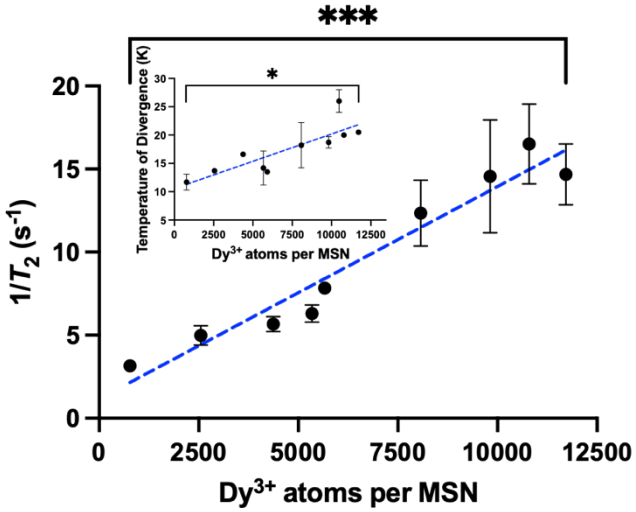

Figure 2. The transverse relaxivity rate ($1/T_2$) recorded at 11.7 T for Dy-doped MSNs spanning a range of loading densities with the relaxation rate shown to increase from 3.16 s^{-1} to 14.68 s^{-1} as the Dy^{3+} concentration is increased (two-tailed t-test, ***, P = 0.0004). The insert shows the temperature of divergence measurements recorded for the Dy-MSNs, taken as the point at which there is a divergence from the same mass susceptibility for the range of recorded frequencies. An increase in the divergence temperature, and hence an indication of increased spin-spin interactions, can be observed as the paramagnet loading density is increased (two-tailed t-test, *, P < 0.05).

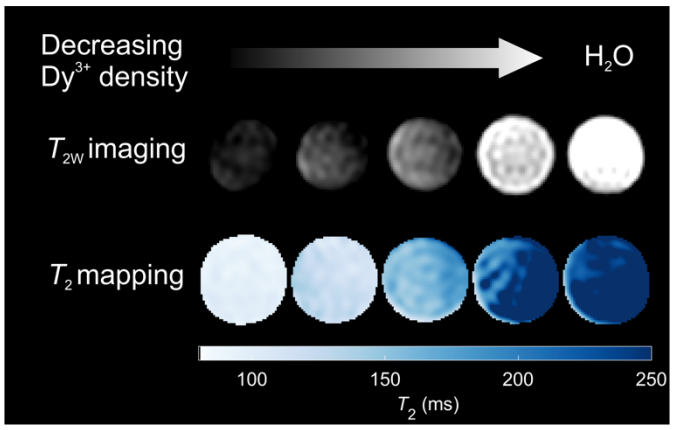

Figure 3. T_2 weighted MRI images recorded at 7 T for a 1 mg mL^{-1} solution of Dy-doped MSNs on a Magnex/Varian DDR2 preclinical MRI system. Phantom mapping of the Dy-doped MSNs arranged by increasing Dy^{3+} loading from 2500 Dy^{3+} MSN^{-1} to 10,000 Dy^{3+} MSN^{-1} can be seen above. The data fitted to an appropriate signal model can be seen below. For both T_2 maps there is an observed darkening in signal intensity/image contrast as the Dy^{3+} concentration is increased.

loading density on image contrast on a 7 T preclinical MRI scanner (Figure 3). A clear influence of Dy^{3+} doping density on image contrast is evident in T_2-weighted images. A quantification of this with T_2 mapping reveals an associated T_2 reduction by ~ 66% as Dy loading per particle increases from 2500 Dy^{3+} MSN^{-1} to 10,000 Dy^{3+} MSN^{-1}, mirroring the scaling Curie effects as resolved at 11.7 T (Figure 2). To rule out any influence of varying Dy-DOTA densities on water accessibility, the isotropic apparent diffusion coefficient (D_{eff}) was recorded for each sample (ESI 9) and observed to be constant within 5 % of the mean reported value across all samples.

To summarise, Dy-MSNs present a chemically tailorable means of supporting effective high field MR imaging. This work has demonstrated that the dominant Curie contributions to image contrast at high scanner fields can be synthetically tuned, and reports, for the first time, the influence of paramagnetic loading density within a nanoparticle scaffold on T_2 contrast. Specifically, intraparticle Dy-Dy interactions increase with doping density, as resolved by AC SQUID analyses, and the contrast generating Curie response scales accordingly and in a manner that enables effective high field imaging.

Acknowledgements

The authors would like to thank Professor Mike Hayward and Dr Simon Cassidy, University of Oxford, Department of Chemistry, for their assistance in SQUID measurements. The authors thank Professor Damian Tyler, University of Oxford, Department of Physiology, Anatomy and Genetics, for assistance in MR imaging acquisition and Daohe Yuan, University of Oxford, Department of Chemistry, for helpful discussions. JJM would like to acknowledge support from the Novo Nordisk Foundation (NNF21OC0068683) from the British Heart Foundation (RE/08/004).

Conflicts of interest

There are no conflicts to declare.

Notes and references

1 J. Wahsner, E. M. Gale, A. Rodríguez-Rodríguez and P. Caravan, *Chem. Rev.*, 2019, 119, 957–1057.
2 D. Ni, W. Bu, E. B. Ehlerding, W. Cai and J. Shi, *Chem. Soc. Rev.*, 2017, 46, 7438–7468.
3 T. H. Shin, Y. Choi, S. Kim and J. Cheon, *Chem. Soc. Rev.*, 2015, 44, 4501–4516.
4 P. Fries, J. N. Morelli, F. Lux, O. Tillement, G. Schneider and A. Buecker, *Wiley Interdiscip. Rev. Nanomedicine Nanobiotechnology*, 2014, **6**, 559–573.
5 P. Caravan, C. T. Farrar, L. Frullano and R. Uppal, *Contrast Media Mol. Imaging*, 2009, **4**, 89–100.
6 Z. Zhou and Z. R. Lu, *Wiley Interdiscip. Rev. Nanomedicine Nanobiotechnology*, 2013, 5, 1–18.
7 G. A. Pereira, J. A. Peters, F. A. Almeida Paz, J. Rocha and C. F. G. C. Geraldes, *Inorg. Chem.*, 2010, **49**, 2969–2974.
8 P. Caravan, M. T. Greenfield and J. W. M. Bulte, *Magn. Reson. Med.*, 2001, **46**, 917–922.
9 L. Vander Elst, A. Roch, P. Gillis, S. Laurent, F. Botteman, J. W. M. Bulte and R. N. Muller, *Magn. Reson. Med.*, 2002, **47**, 1121–1130.
10 E. Debroye, S. Laurent, L. Vander Elst, R. N. Muller and T. N. Parac-Vogt, *Chem. - A Eur. J.*, 2013, **19**, 16019–16028.
11 T. C. Soesbe, S. J. Ratnakar, M. Milne, S. Zhang, Q. N. Do, Z. Kovacs and A. D. Sherry, *Magn. Reson. Med.*, 2014, **71**, 1179–1185.
12 J. Pellico, C. M. Ellis and J. J. Davis, *Contrast Media Mol. Imaging*, 2019, **2019**, 1–13.
13 D. González-Mancebo, A. I. Becerro, T. C. Rojas, M. L. García-Martín, J. M. de la Fuente and M. Ocaña, *Part. Part. Syst. Charact.*, 2017, **34**, 1700116.
14 X. Shi, K. Liu, T. Wang, S. Zheng, W. Gu and L. Ye, *RSC Adv.*, 2016, **6**, 99339–99345.
15 K. Kattel, J. Y. Park, W. Xu, H. G. Kim, E. J. Lee, B. A. Bony, W. C. Heo, S. Jin, J. S. Baeck, Y. Chang, T. J. Kim, J. E. Bae, K. S. Chae and G. H. Lee, *Biomaterials*, 2012, **33**, 3254–3261.
16 G. K. Das, N. J. J. Johnson, J. Cramen, B. Blasiak, P. Latta, B. Tomanek and F. C. J. M. Van Veggel, *J. Phys. Chem. Lett.*, 2012, **3**, 524–529.
17 X. Y. Zheng, J. Pellico, A. A. Khrapitchev, N. R. Sibson and J. J. Davis, *Nanoscale*, 2018, **10**, 21041–21045.
18 H. Hu, Y. Zhang, S. Shukla, Y. Gu, X. Yu and N. F. Steinmetz, *ACS Nano*, 2017, **11**, 9249–9258.
19 D. Yuan, C. M. Ellis and J. J. Davis, *Materials (Basel).*, 2020, **13**, 3795.
20 K. T. Yung, *Magn. Reson. Imaging*, 2003, **21**, 451–463.
21 M. Norek and J. A. Peters, *Prog. Nucl. Magn. Reson. Spectrosc.*, 2011, 59, 64–82.
22 J. D. Satterlee, *Concepts Magn. Reson.*, 1990, **2**, 119–129.
23 I. Bertini, C. Luchinat and G. Parigi, *Prog. Nucl. Magn. Reson. Spectrosc.*, 2002, 40, 249–273.
24 A. J. Vega and D. Fiat, *Mol. Phys.*, 1976, **31**, 347–355.

25 L. Gutiérrez, R. Mejías, D. F. Barber, S. Veintemillas-Verdaguer, C. J. Serna, F. J. Lázaro and M. P. Morales, *J. Phys. D. Appl. Phys.*, 2011, **44**, 255002.
26 M. Bałanda, *Acta Phys. Pol. A*, 2013, **124**, 964–976.
27 R. A. Hein, *Phys. Rev. B*, 1986, **33**, 7539–7549.
28 H. B. G. Casimir and F. K. du Pré, *Physica*, 1938, **5**, 507–511.
29 C. V. Topping and S. J. Blundell, *J. Phys. Condens. Matter*, 2019, **31**, 013001.
30 W. J. Rieter, J. S. Kim, K. M. L. Taylor, H. An, W. Lin, T. Tarrant and W. Lin, *Angew. Chemie Int. Ed.*, 2007, **46**, 3680–3682.

